

Compact LED-Based Displacement Sensing for Robot Fingers

Amr El-Azizi^{*†}, Sharfin Islam^{*†}, Pedro Piacenza^{*†}, Kai Jiang[§], Ioannis Kymissis[‡], Matei Ciocarlie[†]

Abstract—In this paper, we introduce a sensor designed for integration in robot fingers, where it can provide information on the displacements induced by external contact. Our sensor uses LEDs to sense the displacement between two plates connected by a transparent elastomer; when a force is applied to the finger, the elastomer displaces and the LED signals change. We show that using LEDs as both light emitters and receivers in this context provides high sensitivity, allowing such an emitter and receiver pairs to detect very small displacements. We characterize the standalone performance of the sensor by testing the ability of a supervised learning model to predict complete force and torque data from its raw signals, and obtain a mean error between 0.05 and 0.07 N across the three directions of force applied to the finger. Our method allows for finger-size packaging with no amplification electronics, low cost manufacturing, easy integration into a complete hand, and high overload shear forces and bending torques, suggesting future applicability to complete manipulation tasks.

Index Terms—Contact Sensing, LED emitter and receiver, Robot Hand, Robotic Manipulation

I. INTRODUCTION

Detecting the net forces or torques acting on a robotic finger is useful for dexterous manipulation [1]–[5], with the potential to replace or complement tactile sensors. Tactile sensors convey significantly more information, such as the exact location of contact or a pressure map, from which net finger forces can also be extracted. However, tactile sensors offering full fingertip coverage are still not ubiquitous technology. In their absence, information on net forces and torques can still be useful in robot fingers engaged in manipulation tasks.

The most direct method for sensing such forces and torques is to add an off-the-shelf six-axis force and torque (F/T) sensor into the base of the finger. However, such F/T sensors are primarily developed with industrial applications in mind [6]–[8], leading to limitations when being used for dexterous manipulation. Manipulation often benefits from compliance [9], whereas most F/T sensors are optimized to be as stiff as possible, thus requiring precision engineering and leading to a high cost. Industrial applications also tend to favor a higher resolution than is needed for manipulation, but compromise by limiting the overload protection [6]. This leads to sensors that are easily damaged in the uncertain

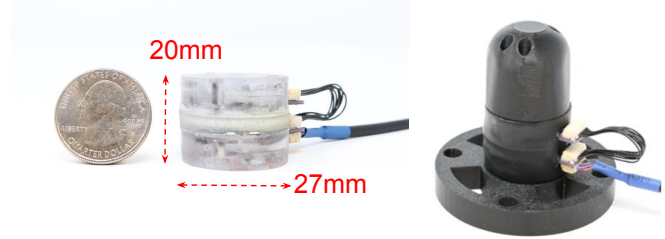


Fig. 1: Our LED-based sensor, standalone (left) and mounted to a fixed base and robot finger (right). We use LEDs mounted on two plates connected by a transparent elastomer to sense displacement between the plates and relate it to applied forces and torques. This method allows for a compact, fully integrated package at a low manufacturing cost.

environments that robotics need to interact with. Finally, off-the-shelf F/T sensors can be difficult to package and integrate into the hand. Others have attempted to solve this problem by designing sensors to be placed within the fingertips [10]–[12]. This limits the geometry of the finger and can also limit the inclusion of other modalities within the finger.

In this paper, we present the design of a displacement sensor intended to provide information about the net forces acting on a robot finger in a manner that addresses the needs of robotic manipulation. First, such a sensor must be easy to manufacture using low-cost components and processes, so that it is affordable and practical to include multiple in a multi-fingered hand. Second, it must have the size and profile suited for the base of a fingertip, which will increase ease of integration into a hand. This also frees up the finger design for alternate sensors, or allows more flexibility in design of a finger. Third, some amount of compliance could be beneficial to manipulation, and thus there is no need to avoid compliance at all cost. Finally, the ideal sensor would have a Signal to Noise Ratio (SNR) that allows it to be useful for manipulation without sacrificing overload protection.

To that end, we develop our sensor based on light transport. Our design, shown in Fig. 1, consists of two plates, connected by an elastomer layer that allows for 6 Degrees of Freedom (DOF) between them. When mounted at the base of a robot finger, any contact force applied to the finger will cause a displacement between these plates. To measure this displacement, we use a network of LEDs on each plate as both light emitters and light receivers. As the plates shift relative to each other due to an externally applied forces, the signal measured by the receiver LEDs changes due to the relative movement and positioning of the emitter LEDs. We record these signals, and use them to extract information

^{*} joint first authorship

[†]Dept. of Mechanical Engineering, [‡]Dept. of Electrical Engineering, [§]Dept. of Computer Science

Columbia University, New York, NY 10027, USA

Email: {aae2155, si2395, pp2511, kj2628, ik2174, mtc2103}@columbia.edu

This work was supported in part by the NSF under awards PFI-232975 and CMMI-2037101.

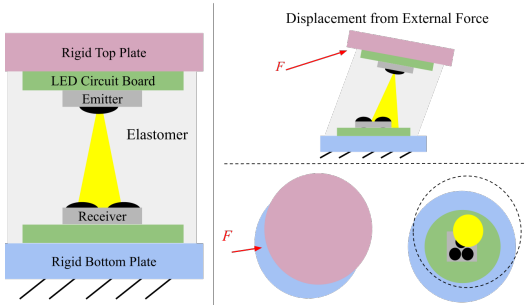


Fig. 2: A diagram of our LED-to-LED sensor concept. We align two PCBs with LEDs directly above each other. We attach these circuit boards to rigid plates, we then suspend both of these plates in a translucent, elastic material. Assuming the bottom plate is fixed, a force applied to the top plate will displace the plate and change how to emitter LED shines on the receiving LEDs. We can then map this change to the contact wrench on the sensor that induced the displacement.

about the forces acting on the finger.

A key feature of our work is that using LEDs as both emitters and receivers confers very high signal-to-noise ratio, significantly higher than using photodiodes. Combined with the small LED form factor, this allows us to sense very small displacements in a compact package. Using an off-the-shelf F/T sensor as ground truth, we show that our sensor has an observed resolution of .06 N and 2.6 N-mm in a compact, low-cost package that is compliant and easy to integrate in robot fingers as it requires no external amplification. To the best of our knowledge, this is the first time that LEDs have been integrated into a 6-DOF flexure, allowing for full contact information in a compact, compliant robot fingers. Our sensor is designed to be integrated at the base of the finger, which allows for sensing coverage of the entire finger and the ability to integrate other sensors in the finger. We hope that this direction can facilitate truly ubiquitous sensing integrated in robot fingers, with future applications in manipulation.

II. RELATED WORK

Many tactile sensors use LEDs due to their compact packaging and wide range of emission cones [13]–[17]. The LEDs in these sensors are embedded in a translucent elastomer, so that their emission cone shines on a receiving device. This receiver is often a photodiode [14], [16] or camera [15], [17], [18], but can also be an LED [19]. Regardless of the receiving device, when a force is applied to the surface of these sensors, the elastomer deforms and the emitter and receiver will displace. Using either a data-driven approach or deriving an analytical relationship, the change in electrical signal from this deformation can then be mapped to the contact applied. These tactile sensors are not able to cover the full surface of a robot finger, and therefore do not provide full sensing coverage all possible contacts. To detect the full contact, others have tried several modalities including strain-based transducers [20], capacitance [21], optical [22], and magnetic [12]. Although most of these sensors are too

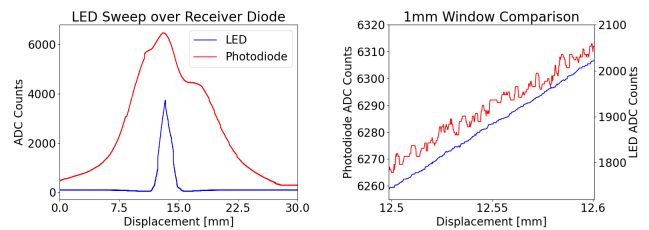


Fig. 3: Graphs showing the sensitivity of LEDs and Photodiodes when used as light receivers. **Left:** This graph shows the sharper cone response of the LED when compared to the photodiode. **Right:** This graph is a zoom in on the ADC signal received across a .1mm window. It shows the clearer SNR when using the LEDs as receivers versus the dedicated photodiodes. Because the signal is spread over a smaller area, there are sharper changes at small displacements, including in a .1 mm window.

large to integrate in a robot finger, there are a few novel F/T sensors that are built particularly for manipulation.

In Table 1, we organize other low-cost sensors developed specifically to address the needs of contact wrench detection in robot fingers. For example, Guggenheim et al. embedded barometers in a rubber flexure and placed them between two rigid plates [23]. These plates are relatively large with the length and width being 75mm. The size is constrained by the number of barometer modules needed to get 6-axis forces and torques. Camera-based sensors are more compact as they only need a single camera module, but require a completely translucent or hollow flexure. Some low-cost F/T sensors use small cameras to track the displacement of a marker fixed on some flexure. Ouyang et al. suspended a fiducial marker above a small camera module, using a compression spring as the flexure [24]. However, this design requires a relatively tall structure at 51mm. The Visiflex, a camera-based F/T sensor developed by Fernandez et al., is much more compact [10]. However, it only tracks forces and torques applied directly on the surface of the sensor. Therefore, contact anywhere else on the manipulator will not be sensed. In contrast, Kim et al. developed a very compact and capable F/T sensor using cylindrical capacitors [11]. The overall package of the sensor is very small, especially compared to the other low-cost sensors listed in Table I. While force range is high, torque range is limiting, as is the absolute accuracy reported.

Overall, we note that different sensors in Table I shine in different respects. In this context, the method introduced in this paper allows for compact size (27mm diameter and 20mm height), high bandwidth (2.5KHz) and good absolute accuracy, a low manufacturing cost (\$100 in small quantities), overload forces up to 110N, and overload torques up to 1.62 N*m. Overall, we believe each of these technologies holds promise for advancing manipulation, and different sensors will suit different use cases and application scenarios.

III. SENSOR DESIGN

A. Concept

Our conceptual diagram of our sensor is shown in Fig. 2. It consists of two rigid plates connected by an elastomeric

Modality	Cost	Size	Min Forces and Torques	Max Forces and Torques	Accuracy (R^2)	Bandwidth
Barometer [23]	\$20	L : 75 mm W : 75mm H : 5 mm	Fx - <0.1N Fy - <0.1N Fz - <0.1N Mx - <0.1Nmm My - <0.1Nmm Mz - <0.1Nmm	Fx - 30 N Fy - 40 N Fz - 10 N (tension) Fz - 10 N (compression) Mx - 40 Nmm My - 40 Nmm Mz - 30 Nmm	Fx - 0.937 Fy - 0.909 Fz - 0.998 Mx - 0.984 My - 0.984 Mz - 0.991	50 Hz
Camera [24]	\$40	L : 35.7mm W : 22.5mm H : 51 mm	Fx - 0.1N Fy - 0.1N Fz - 0.1N Mx - 0.5Nmm My - 0.5Nmm Mz - 0.5Nmm	Fx - 65 N Fy - 18 N Fz - 0.1 N (tension) Fz - 80 N (compression) Mx - 80 Nmm My - 40 Nmm Mz - 4 Nmm mm	Fx - 0.991 Fy - 0.996 Fz - 0.875 Mx - 0.997 My - 0.997 Mz - 0.902	25 Hz
Camera [10]	\$400	L : 35 mm W : 35 mm H : 35 mm	Not reported	Fx - 10 N Fy - 10 N Fz - 0.1 N (tension) Fz - 10 N (compression) Mx - Not reported My - Not reported Mz - Not reported	Fx - 0.993 Fy - 0.980 Fz - 0.988 Mx - 0.986 My - 0.980 Mz - 0.985	40 Hz
Capacitance [11]	\$100	Rad : 14 mm H : 6.5 mm	Fx - 8.1 mN Fy - 10.2 mN Fz - 5.4 mN Mx - .25Nmm My - .23Nmm Mz - .1Nmm	Fx - 30N Fy - 30N Fz - 30N (tension) Fz - 30N (compression) Mx - 0.30 N*m My - 0.30 N*m Mz - 0.30 N*m	absolute: Fx - 0.276 N Fy - 0.249 N Fz - 0.471 N Mx - 4.86 Nmm My - 5.13 Nmm Mz - 1.71 Nmm	200 Hz

TABLE I: Comparison of novel 6-axis sensors developed to extract full contact information in the context of dexterous robot manipulation

layer that allows 6-DOF displacements. The electronics fixed to each rigid plate consist of a circuit boards with emitter LEDs and clusters of receiving LEDs. At the neutral position, the emitter LED is directly above the center of the receiving cluster. When an external force is applied, the plates will displace relative to each other. This displacement will result in a change in signal for the receiver LEDs due to the relative motion of the corresponding emitter LED. We can then map this change in signal back to the contact wrench applied.

B. Analysis of Single Emitter-Receiver Pair

Displacement transduction via light measurements offers three primary advantages. First, it provides a fast response time, as diode readings are gated by the ADC rather than the diodes. Second, its components require minimal space, which aids with reducing our footprint. Third, we can select LEDs in the IR spectrum, making the sensor resistant to the majority of external environment light. Adding an opaque wrapping to the outside of our sensor, we can further prevent any external light interference from external infrared light.

Using LEDs as both a receiver and emitter gives us several advantages over the other modalities mentioned in Table I. First, light can be sensed at very high frequencies with minimal electrical noise. There are several devices we could use as our receiver, but we opted to use LEDs as the receivers. In our case, the decision of using receiving LEDs over photodiodes was made based on 3 factors. 1) LEDs have a smaller form factor than most photodiodes in the price range. 2) LEDs are optimized for operation in their wavelength range, making it easier to design features

to minimize external interference. 3) LEDs have a smaller viewing angle, which is useful for increasing sensitivity given our size constraints.

We first verify the validity of LEDs as both emitters and receivers, and compare to the alternative using photodiodes on the receiving end. To that end, we measured the response to relative horizontal displacements of a single emitter-receiver pair separated by an air gap, where the receiver consisted of either an LED or a photodiode. The results, plotting receiver signal vs. relative horizontal displacement of the emitter, are shown in Fig. 3. We observe that the LED receiver exhibits much higher sensitivity compared to its photodiode counterpart. In fact, the LED receiver can identify displacements as small as 0.01 mm, whereas the corresponding signal changes for a photodiode receiver are comfortably inside the noise level. Based on this result, we proceed with LED-LED pairs for the overall sensor design.

C. Complete Sensor Design

With the core concept of using identical LEDs as emitters and receivers verified, we implemented a preliminary design for the sensor. As we wanted to mount this at the base of a finger, we constrained our design to a 1 inch (25.4 mm) diameter. The goal was to maximize the amount of data signals within the space. Based on our LED analysis, we used a compact, infrared LED (SFH 4056) with an emission cone of 20° . The primary size constraint became the op-amps, which meant we could support a maximum of 12 signals per board. As shown in the left of Fig. 4, we divided the signals into clusters of 4 receivers, so that each board had 3 clusters,

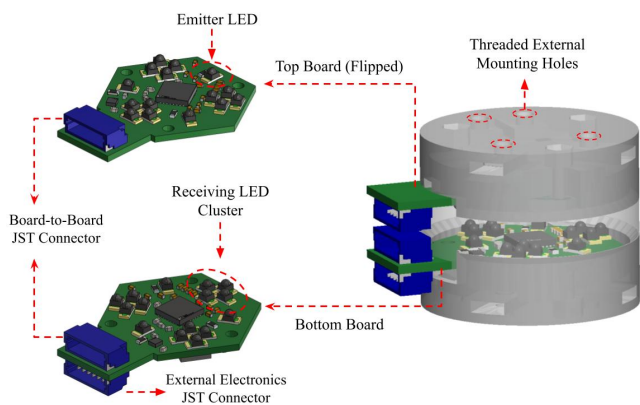


Fig. 4: Our sensor is composed of two custom PCBs that have both LED emitters and clusters of LED receivers. When the top and bottom PCB boards are aligned facing each other, our sensor has 3 total emitter-receiver pairs. The PCBs are fastened to rigid, 3-D printed plates. The plates are then fixed above each other in a mold that we then fill with PDMS and cure to get the sensor on the right. We use a single JST connector to communicate between the top and bottom board. We use an additional JST connector on the bottom board to communicate with external electronics. The rigid plates are fitted with threaded holes to mount external hardware. Our sensor is 27 mm in diameter, 20mm in height, and weighs 16.4g.

for a total of 24 signals broken across 12 clusters. We then suspended the PCB boards above each other and attached them with an elastic flexure.

We fastened the bottom and top PCB boards, as shown in Fig. 4, each to a rigid, 3-D printed plate. The plates each have three M2 inserts that we can mount external hardware too. We used these inserts to attach these rigid plates to a mold that we then filled with an uncured mixture of PDMS. We cured the filled mold at $70^{\circ}C$ for 8 hours, which gave us the sensor shown in Fig. 4. The overall dimensions of the sensor is 20.82mm in height and a diameter of 27mm, which is just above our target diameter. We then covered the sensor with a thin, opaque rubber shrink-wrap tube. This cover inhibits interference from external light sources, but also helps adds to the sensor robustness. We cured the PDMS at a 10:1 ratio of base to curing agent, as we observed this best achieved the desired sensor stiffness and surface finish. Moreover, this ratio produced the most consistent behavior across multiple sensors.

To increase PDMS adherence to the plates, we treated the PCB boards with silicone primer to promote strong adhesion between the PDMS and PCB faces. We also added a lip to the rigid plates that extends past the PCB surface to help the PDMS from shearing off the PCB. The rubber wrapping also increases the stiffness of our sensor and adds robustness under large displacements, especially in shear.

Our electronics also need to take into account concerns with integration in a robot hand. To that end, we want to minimize the number of signals transmitted between the board and the controller. Using an on-board ADC provides four advantages: 1) It allows for higher quality signals than

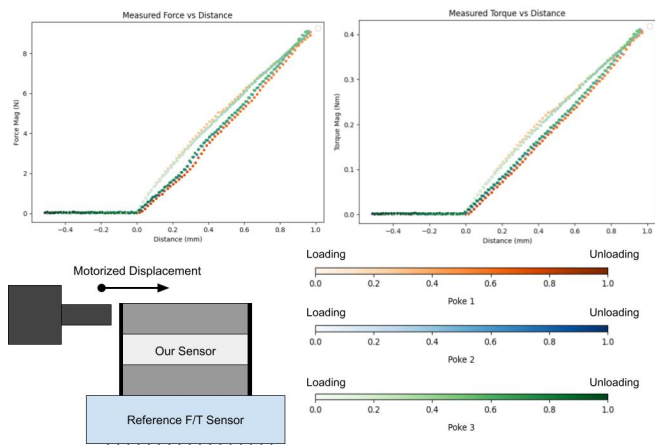
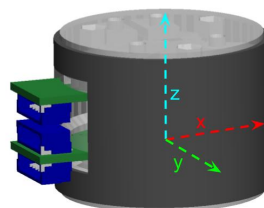


Fig. 5: Mechanical hysteresis testing over three consecutive loading and unloading cycles. We fixed our sensor, with its rubber cover, on a reference F/T sensor and then used a linear probe to displace the top plate by 1 mm. Plotting the force and torque vs displacement for three consecutive cycles of pokes, we observe some hysteresis that is relatively consistent between cycles.



Failure Mode	Force/Torque Direction	Failure Magnitude
Shear	F_x, F_y	110.8 N
Bending	M_x, M_y	1.62 N*m
Torsion	M_z	1.06 N*m
Tension	F_z (positive)	65.8 N
Compression	F_z (negative)	>200 N

Fig. 6: Mechanical overload forces and torques for our sensor. We built five sensors and then used an ADMET instron machine to apply a horizontal force until the sensor failed. By fixing it to the machine in different ways, we tested our sensor in five major failure modes - shear, bending, torsion, tension, compression. All tests were done with the opaque, shrink wrapped rubber cover on. Our sensor does not break under very high forces and torques, which is ideal for contact rich manipulation in uncertain robot environments.

utilizing the built-in ADCs on the micro-controller. 2) It allows us to use SPI protocol with only 7 wires. This also enables chaining of the top plate and bottom plate of the sensor using the SPI protocol. 3) It allows us to only transmit digital signals across the cables, minimizing transmission noise. 4) We maintain higher response time by avoiding external multiplexing.

IV. MECHANICAL CHARACTERIZATION

A core design objective of this sensor is robustness against large displacements induced by high contact forces. We tested our sensor to failure in five failure modes - shear, bending, torsion, tension, and compression. We note that, since our sensor is intended to be mounted at the base of a finger, as shown in Fig. 1, contact forces will mostly cause shear and bending of our sensor. Additionally, all tests on our sensor were done with a shrink wrapped neoprene cover, as shown on the finger in Fig. 1. This cover improved the robustness of our sensor, as it added an extra layer of protection to the PDMS flexure, especially for shear and

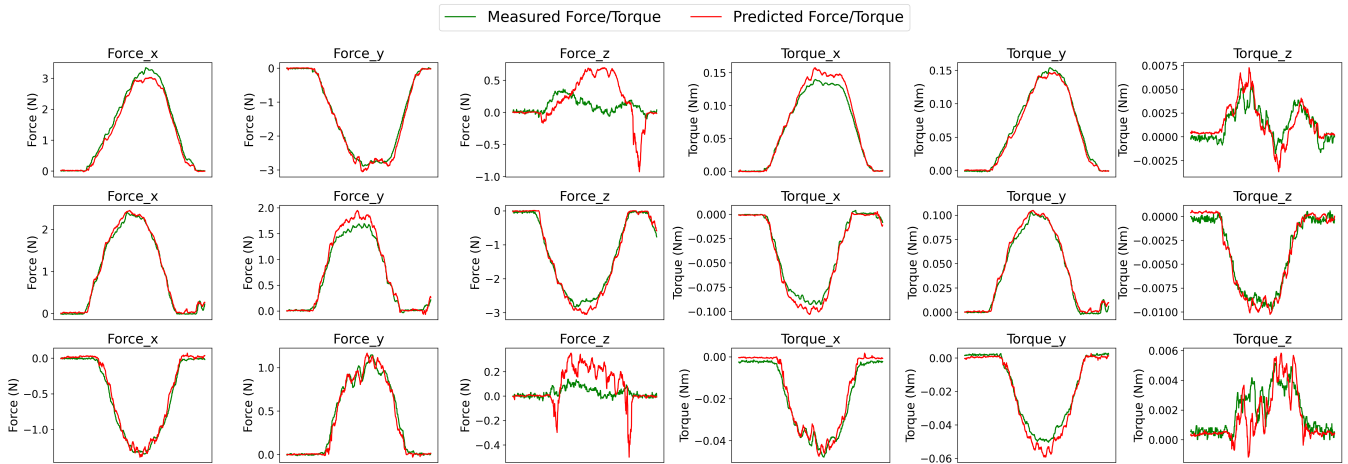


Fig. 7: Predicted vs. ground truth forces and torques across all 6 DoFs. Each row represents a test poke on our sensor. The contact prediction model demonstrates strong performance for forces and torques along/about the x and y-axes but struggles particularly with force prediction along the z-axis.

tension forces.

The magnitude and direction of the forces and moments for each failure mode relative to our sensor are shown in Fig. 6. In particular, we note that our sensor withstands shear forces of up to 110 N and bending torques of up to 1.62 N*m. The overload forces for torsion and compression are also high. Our sensor is weakest in tension, which is not a major concern as a robot finger would likely not experience large tension forces while doing manipulation in uncertain environments.

PDMS is a hysteric material, so we expect our 6-DOF flexure to display some time-dependent non-linearity [13], [25]. In Fig. 5, we plot the results of cyclic loading and unloading tests for our sensor. We used a linear probe to horizontally displace the top plate of our sensor while it was fixed to a reference, off-the-shelf F/T sensor. Displacing the top plate by 1 mm three consecutive times, we observe hysteresis that is relatively consistent over the cycles. While hysteresis is a common effect for sensors that use PDMS as an elastic flexure [25], it is also problematic for mapping the electrical signals to the force applied, and often displays behavior that is unique to each sensor. In future work, we aim to investigate different clear elastomers for reducing this effect, potentially in combination with more complex learning architectures that can aim to learn this behavior and reduce in post processing.

V. PERFORMANCE

In this section, we aim to quantify the performance of our design as a standalone sensor. Ultimately, we believe that the true value of a sensor designed for robot fingers lies in the performance improvements it enables for complete manipulation. If manipulation is performed via learned policies, such policies are likely to use raw sensor data as input (in our case, raw readings from the receiver LEDs), decreasing the importance of any intermediate representations. However, training such a policy exceeds the scope of this paper, which focuses on the design of the sensor itself.

Therefore, in order to quantify the standalone performance of our sensor, we test the ability to infer ground truth wrenches applied to the robotic finger from the raw sensor data. To that end, we mount our sensor on a commercial ATI SI-130-10 to obtain ground truth force and torque measurements. We then trained a simple machine learning model to predict applied force and torque based on our sensor data. We describe the experimental approach and results in this section.

A. Data Collection

To collect the dataset, we mounted a 3D-printed finger-like shape on top of our sensor, as shown on the right in Figure 1. We made contact with it from all directions along its circumference. Each data file contains three contact events recorded within a 15-second span. To ensure force and torque were decoupled, we applied a range of forces at different heights. The dataset primarily captures forces between 0–5 N and torques between 0–0.2 Nm along each axis, with a maximum force magnitude limited to under 10 N.

We selected 10 contact locations, distributed evenly around the circumference of the finger. Contacts were applied by pressing against the printed finger with our fingertip for 2 and 5 seconds. For the training set, we collected data for 15 different contacts at each location. These contacts were grouped into sets of three, each recorded at different heights—top, middle, and bottom of the finger. Each set focused on a specific force range to ensure comprehensive coverage. The test sets are collected with the same procedure, but included only 1 contact per surface for each contact position. The test set was randomly split across the height groupings to be representative of the different torque-force pairings.

During data collection, the sensor operated at a sampling rate slightly above 2.5 kHz. However, data was down-sampled and recorded at 250 Hz due to the practical requirements of robotic manipulation tasks.

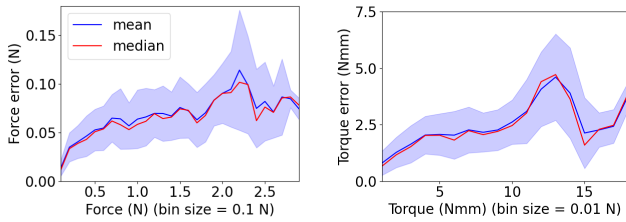


Fig. 8: Graphs of error plotted against magnitude of the signal. **Left:** Force. **Right:** Torque. The plots demonstrate that for both force and torque, the magnitude of error scales slower than the magnitude of the force. What starts at a 20% mean error rapidly becomes a 5-10% mean error after 1N of force.

B. Data pre-processing

Prior to training, we applied a series of pre-processing techniques to improve data quality and model performance. To reduce high-frequency noise, we used an 11-point median filter on the raw sensor readings and a 5-point median filter on the ground truth data. Given our data collection rate of 250 Hz, this filtering process introduces a delay of less than 0.1 seconds, which is negligible for our application.

To distinguish between contact and non-contact states, we thresholded all data points with a total force magnitude below 0.1 N as “no contact.” However, to prevent the dataset from being overwhelmingly dominated by these points, we downsampled them to ensure they constitute only 10% of the training data.

Additionally, instead of training directly on absolute raw signals, we extracted features based on their relative changes from a no-contact baseline. This baseline was defined as the mean of the first 50 data points in each recorded dataset. To further stabilize training and maintain numerical consistency, we normalized all features and labels prior to training. These pre-processing steps help the model focus on signal variations rather than absolute values, enhancing generalization.

C. Learning Algorithms

For all experiments on the sensor, we employ an updated ResNet-based architecture inspired by He et al. [26]. Our model consists of a shared feature extraction backbone followed by six independent task-specific heads, one for each of the six DOFs in force and torque prediction.

The key component of our model is the residual block with 1D convolutional layers. Each residual block integrates 1D convolutional layers, skip connections and ReLU activation functions to enhance feature extraction while mitigating vanishing gradients.

The input to the model is a 24-channel time-series sequence, corresponding to the preprocessed sensor signals. A 1D convolutional layer with an enlarged kernel is applied before the residual blocks to capture global patterns in the sensor signals. This is followed by a shared backbone, which is a 1D ResNet specifically designed for sequential sensor data. The backbone consists of multiple residual blocks that efficiently capture spatial and temporal dependencies.

Variable	Mean Abs. Error	Std. Dev.	R ²
Force x (N)	.0560	.0714	.990
Force y (N)	.0533	.0687	.993
Force z (N)	.0690	.0890	.560
Force magnitude (N)	.0640	.0801	.978
Torque x (Nmm)	2.62	3.45	.995
Torque y (Nmm)	2.68	3.41	.991
Torque z (Nmm)	.636	.730	.923
Torque magnitude (Nmm)	2.90	3.85	.986

TABLE II: Accuracy Reporting for the F/T Model. X, Y, and magnitude results are quite promising, but Z still requires further data collection and training before conclusions can be drawn. Despite the absolute error being in the same threshold, the magnitude of Z forces is much smaller leading to a higher percentage error. This is most evident in the R2 results which shows the much higher correlation for x and y than for z

After the shared backbone, the model branches into six independent prediction heads, each dedicated to estimating a specific force or torque component. Each head consists of additional residual layers, a global average pooling layer, and a fully connected output layer that generates a single scalar value. This multi-task learning framework enables specialized feature extraction while leveraging shared representations, thereby enhancing generalization across different force and torque components.

The model is trained using a mean squared error (MSE) loss function, applied separately to each output head. Training is conducted for 100 epochs using the Adam optimizer with a batch size of 2048 and an initial learning rate of 1e-3, which is adjusted dynamically using a LambdaLR scheduler.

D. Results and Discussion

The overall results of our sensor’s contact prediction are presented in Table II and Figure 8. In particular, Table II details the performance for each force and torque direction, as well as the overall force and torque magnitudes. Figure 8 visualizes the mean absolute error as a function of applied force and torque. In addition, Figure 7 provides a detailed performance analysis, showcasing all six force/torque dimensions across three exemplar contacts, each differing in the contact positions. We note again that the test data consisted of contacts never seen in training.

We observe that the sensor provides accurate measurements in both force and torque for the x and y axes, but less so for the z axis. Noise levels are generally low, and predictions are accurate in terms of overall force magnitude, but can occasionally suffer from accuracy at higher forces in individual DOFs. The model was evaluated primarily on the 0-5 N range of forces, but experimentation showed that training on data that extended beyond this range proved useful for the models learning.

We believe that one likely source of error is hysteresis introduced by the PDMS and quantified in Sec. IV. This is particularly prevalent with larger forces, where signals will take some time to settle back to their baselines, which introduces noise to forces done before the resettling. It also introduces noise into the zero-force data.

VI. CONCLUSION AND FUTURE WORK

In this paper, we introduce a low-cost, compliant sensor designed to be easily integrated in a robot finger and provide information on the displacement induced by contact with the world. Our method relies on sensing the displacement between two rigid plates, each mounted with LED emitters and receivers. We analyzed such an LED-LED pair in isolation, and found it to be highly sensitive to relative displacements of the emitter and the receiver. We thus designed a sensor with six LEDs acting as emitters and 24 LEDs acting as receivers, distributed between the top and bottom plates of the sensor.

To characterize the information contained in the raw signals from our sensor, we tested whether it is possible to reconstruct overall finger wrench information, using a commercial force/torque sensor as ground truth. Our results showed that a simple supervised learning model trained on data from the 24 receiver LEDs can learn to map changes in these signals due to displacement of the flexure to external forces and torques applied between the two plates. The sensor output was particularly accurate for force/torques along/around the x and y axes, with additional work needed to improve sensitivity for the z axis.

Although our sensor does not outperform the accuracy or precision of commodity F/T sensors, we believe that it offers useful information - especially along/about the axes most prevalent for manipulation - in a compact, robust and low-cost package. Modern learning-based manipulation methods often operate directly on raw, even uncalibrated sensor data [27], [28], thus converting to an intermediate representation such as the one used here for sensor characterization may be unnecessary in the future. Considering the strong SNR of the raw signals of our sensor, we believe that it can be used in a similar manner for policy learning for manipulation.

Future work of the sensor falls under two categories: further improvement of the sensor, and implementation within actual use robot hands. Sensor improvement in turn will have mechanical, electronic, and learning components. Mechanically, we would like to reduce hysteresis, simplify the manufacturing, and improve the consistency between sensors. We would also like to reduce the stiffness in the z-axis so that we get more sensitivity in that direction. Electronically, we will continue to look for sources of noise in LED signals. We also want to minimize the form factor as much as possible, so further experiments would include use of fewer LEDs in each cluster (or potentially even fewer clusters). Learning wise, we will further tune the model as we gather more data for Z axis and explore alternate architectures with both time series and single-snapshot models.

We look to take advantage of the features of the sensor which make it particularly attractive for integration in robot hands. In particular, the form factor and ease of integration (the sensor directly connects to a micro-controller board with no additional amplification electronics) are highly appealing. Figure 9 shows a possible design of an anthropomorphic hand with one of our sensors at the base of the distal phalanx



Fig. 9: A render of an anthropomorphic hand design with the F/T sensors proposed in this paper mounted at the base of every finger.

of each finger. Such integration will also allow us to test the hypothesis that slight compliance in the sensing element can prove beneficial, or at least non-detrimental, to dexterous manipulation.

As motor learning for dexterous manipulation makes continuous advances, we believe that sensing will prove key for future performance of robot hands. Having a multitude of sensors at our disposal, each with various strengths, will increase the ability of combining the right sensor with the right motor learning method to achieve novel capabilities. We believe that the sensor presented in this paper represents a step in this direction.

REFERENCES

- [1] L. Gao, P. Lee, and R. Bai, "Learning dexterous manipulation from human demonstrations for robotic in-hand manipulation tasks," *IEEE Robotics and Automation Letters*, vol. 5, no. 2, pp. 3015–3022, 2020.
- [2] H. Liu, Z. Li, and D. Sun, "Multi-sensory robotic systems for dexterous manipulation: A survey," *IEEE/ASME Transactions on Mechatronics*, vol. 24, no. 2, pp. 457–470, 2019.
- [3] J. Maurice, P. Letier, F. Flacco, and A. De Luca, "Machine learning techniques for estimating object manipulation forces from force/torque sensor data," in *Proceedings of the 2022 IEEE International Conference on Robotics and Automation (ICRA)*, 2022, pp. 5600–5606.
- [4] O. Leslie, D. Córdova Bulens, and S. J. Redmond, "Design, fabrication, and characterization of a novel optical six-axis distributed force and displacement tactile sensor for dexterous robotic manipulation," *Sensors*, vol. 23, no. 24, p. 9640, 2023.
- [5] S. Pirozzi, G. Carbone, and F. Mangione, "Design and calibration of a force/tactile sensor for dexterous manipulation," *Sensors*, vol. 19, no. 4, p. 966, 2019.
- [6] A. Jafari and N. G. Tsagarakis, "Force/torque sensors: From industrial robotics to human-robot interaction," *IEEE Robotics and Automation Magazine*, vol. 27, no. 2, pp. 34–43, 2020.
- [7] K. Min, F. Ni, and H. Liu, "An efficient and accurate force/torque sensing method based on an excitation trajectory," *Industrial Robot*, vol. ahead-of-print, 2023.
- [8] D. Yamamoto, S. Shirogane, and S. Sugano, "Development of force/torque sensor with omni-directional multi-axis load detection for dexterous robotic hands," *Sensors and Actuators A: Physical*, vol. 317, p. 112478, 2021.
- [9] R. Chi and A. Dollar, "On dexterity and dexterous manipulation," *Frontiers in Robotics and AI*, 2021.
- [10] A. J. Fernandez, H. Weng, P. B. Umbanhowar, and K. M. Lynch, "Visiflex: A low-cost compliant tactile fingertip for force, torque, and contact sensing," *IEEE Robotics and Automation Letters*, vol. 6, no. 2, pp. 3009–3016, 2021.
- [11] U. Kim, H. Jeong, H. Do, J. Park, and C. Park, "Six-axis force/torque fingertip sensor for an anthropomorphic robot hand," *IEEE Robotics and Automation Letters*, vol. 5, no. 4, pp. 5566–5572, 2020.

- [12] T. Le Signor, N. Dupré, J. Didden, E. Lomakin, and G. Close, "Mass-manufacturable 3d magnetic force sensor for robotic grasping and slip detection," *Sensors*, vol. 23, no. 6, 2023. [Online]. Available: <https://www.mdpi.com/1424-8220/23/6/3031>
- [13] J. Yin, Y. Luo, L. Chen, Q. Wang, H. Yu, and K. H. Li, "High-resolution optical three-axis tactile microsensor based on iii-nitride devices with integrated pdms bumps," *IEEE Electron Device Letters*, vol. 44, no. 12, pp. 2035–2038, 2023.
- [14] D.-H. Jeong, J.-U. Chu, and Y.-J. Lee, "Development of knu hand with infrared led-based tactile fingertip sensor," in *2008 International Conference on Control, Automation and Systems*, 2008, pp. 1156–1161.
- [15] W. Yuan, S. Dong, and E. H. Adelson, "Gelsight: High-resolution robot tactile sensors for estimating geometry and force," *Sensors (Basel, Switzerland)*, vol. 17, 2017. [Online]. Available: <https://api.semanticscholar.org/CorpusID:3474913>
- [16] P. Piacenza, K. Behrman, B. Schifferer, I. Kymissis, and M. Ciocarlie, "A sensorized multicurved robot finger with data-driven touch sensing via overlapping light signals," *IEEE/ASME Transactions on Mechatronics*, vol. 25, no. 5, pp. 2416–2427, 2020.
- [17] D. Ma, E. Donlon, S. Dong, and A. Rodriguez, "Dense tactile force estimation using gelslim and inverse fem," in *2019 International Conference on Robotics and Automation (ICRA)*, 2019, pp. 5418–5424.
- [18] Y. Zhang, Z. Li, X. Zhang, X. Liu, S. Zhang, and W. Chen, "Gelsight360: An omnidirectional camera-based tactile sensor for dexterous robotic manipulation," *IEEE Robotics and Automation Letters*, vol. 6, no. 4, pp. 6458–6465, 2021. [Online]. Available: <https://ieeexplore.ieee.org/document/9346350>
- [19] J. Rossiter and T. Mukai, "A novel tactile sensor using a matrix of leds operating in both photoemitter and photodetector modes," in *SENSORS, 2005 IEEE*, 2005, pp. 4 pp.–.
- [20] P. Billeschou, C. Albertsen, J. C. Larsen, and P. Manoonpong, "A low-cost, compact, sealed, three-axis force/torque sensor for walking robots," *IEEE Sensors Journal*, vol. 21, no. 7, pp. 8916–8926, 2021.
- [21] U. Kim, D.-H. Lee, Y. B. Kim, D.-Y. Seok, and H. R. Choi, "A novel six-axis force/torque sensor for robotic applications," *IEEE/ASME Transactions on Mechatronics*, vol. 22, no. 3, pp. 1381–1391, 2017.
- [22] G. Palli, L. Moriello, U. Scarcia, and C. Melchiorri, "Development of an optoelectronic 6-axis force/torque sensor for robotic applications," *Sensors and Actuators A: Physical*, vol. 220, pp. 333–346, 2014. [Online]. Available: <https://www.sciencedirect.com/science/article/pii/S092442471400418X>
- [23] J. W. Guggenheim, L. P. Jentoft, Y. Tenzer, and R. D. Howe, "Robust and inexpensive six-axis force–torque sensors using mems barometers," *IEEE/ASME Transactions on Mechatronics*, vol. 22, no. 2, pp. 838–844, 2017.
- [24] R. Ouyang and R. D. Howe, "Low-cost fiducial-based 6-axis force–torque sensor," in *2020 IEEE International Conference on Robotics and Automation (ICRA)*. IEEE, 2020, pp. 1653–1659.
- [25] F. Schneider, J. Draheim, R. Kamberger, and U. Wallrabe, "Process and material properties of polydimethylsiloxane (pdms) for optical mems," *Sensors and Actuators A: Physical*, vol. 151, no. 2, pp. 95–99, 2009. [Online]. Available: <https://www.sciencedirect.com/science/article/pii/S0924424709000466>
- [26] K. He, X. Zhang, S. Ren, and J. Sun, "Deep residual learning for image recognition," in *Proceedings of the IEEE conference on computer vision and pattern recognition*, 2016, pp. 770–778.
- [27] R. Bhirangi, V. Pattabiraman, E. Erciyas, Y. Cao, T. Hellebrekers, and L. Pinto, "Anyskin: Plug-and-play skin sensing for robotic touch," 2024. [Online]. Available: <https://arxiv.org/abs/2409.08276>
- [28] V. Pattabiraman, Y. Cao, S. Haldar, L. Pinto, and R. Bhirangi, "Learning precise, contact-rich manipulation through uncalibrated tactile skins," 2024. [Online]. Available: <https://arxiv.org/abs/2410.17246>